PCB Diffusion in concrete and sand
Edmund Crouch, Ph.D.
January 5, 2019

Diffusion of PCBs in concrete

There are few attempts to measure PCB diffusion into concrete. The only published direct approach, with measurements of PCB concentrations at various depths into concrete exposed for 40 years, is that of Liu *et al*. (2015). Unfortunately, these authors used a slightly incorrect physical model, and then used a mathematical approximation that they admitted was invalid for concrete. Fortunately, both problems are relatively easy to correct; and since the original measurements were published in supplemental information, it is straightforward to apply a correct analysis.

Liu *et al*. (2015) measured concentrations of 6 PCB congeners at depths up to 5 cm (approximately) into concrete that had been in contact with a PCB-containing caulk material for 40 years. The caulk was applied between door jambs and concrete walls, or between concrete wall panels, and in Liu *et al*. (2015), and here, it is assumed that the dimensions of the caulk in contact with the concrete were sufficient that a one-dimensional approximation is adequate for modeling.[1] For PCB diffusion into concrete, the mathematical model adopted by Liu *et al*. (2015) for each of the congeners was for one-dimensional diffusion:

$$\frac{\partial C}{\partial t} = D\frac{\partial^2 C}{\partial x^2} \tag{1}$$

where C is the concentration (mass/unit volume)[2] of the congener in the concrete at time t and depth x into the concrete, and D is the diffusivity of the congener in the concrete. Fully specifying such a model requires also specifying the boundary conditions for the differential equation, and the boundary conditions adopted were:

$$\begin{gathered} C(x, t = 0) = 0 \\ C(x = 0,\ \text{all}\ t) = C_m/K \\ \left.\frac{\partial C}{\partial x}\right|_{x=L} = 0 \end{gathered} \tag{2}$$

The first boundary condition corresponds to an initially uncontaminated concrete, and the second to the surface of the concrete being at a constant concentration, equal to $1/K$ times the measured concentration C_m in the caulk (where K is a partition coefficient). The third indicates zero PCB flux at some depth L into the concrete – *i.e.* an impermeable barrier at depth L in the concrete. Nothing in the description of the physical situation, however, corresponds to such an impermeable barrier. The correct boundary condition for the situation described corresponds to zero concentration (or equivalently zero flux) at an (effectively) infinite depth. Fortunately, this discrepancy is easily fixed in the following analysis by taking the limit as L tends to infinity.

Defining dimensionless parameters

[1] This strictly required caulk dimensions parallel to the concrete greater than about 5 cm, but these dimensions were not specified.
[2] In practice, all the measurements are of mass fractions rather than concentrations; but this is irrelevant to the analysis since everything is referred to the concrete which is assumed to have constant density. The caulk-concrete partition coefficients (K) given here are ratios of mass fractions.

Green Toxicology LLC www.GreenToxicology.com 781-316-1685 Crouch@GreenToxicology.com

$$\begin{aligned}\alpha &= x/L \quad \text{so } 0 \leq \alpha \leq 1 \\ \gamma &= \sqrt{\frac{Dt}{L^2}} \quad \text{so } \gamma \geq 0\end{aligned} \tag{3}$$

the solution to the mathematical model posed above is given by (see Appendix 1)

$$\begin{aligned}C(x,t) &= \frac{C_m}{K}\left\{1 - 2\sum_{n=1}^{\infty}\frac{\sin\big((n-0.5)\pi\alpha\big)\exp(-(n-0.5)^2\pi^2\gamma^2)}{(n-0.5)\pi}\right\} \\ &= \frac{C_m}{K}\left\{\operatorname{erfc}\left(\frac{\alpha}{2\gamma}\right) + \sum_{n=1}^{\infty}(-1)^n\left[\operatorname{erfc}\left(\frac{n+\alpha/2}{\gamma}\right) - \operatorname{erfc}\left(\frac{n-\alpha/2}{\gamma}\right)\right]\right\}\end{aligned} \tag{4}$$

where the first series is best for numerical computation at large values of $\sqrt{(Dt)}/L$, and the second for small values of $\sqrt{(Dt)}/L$.

In their exposition, Liu *et al*. (2015) used an approximation to the first of these series, which approximation is invalid for almost all of the concrete measurements.[3] In the limit of L becoming infinite, which corresponds most closely to the concrete measurements of Liu *et al*. (2015) with no impermeable barrier, the infinite sum vanishes in the second series, leaving just a single complementary error function (erfc) term (as may also be obtained by direct solution of the differential equation with the correct boundary conditions). The ratio α/Υ remains finite as L becomes infinite, even though both α and Υ vanish.

Liu *et al*. (2015) in their supplemental information provide concentration measurements for the six congeners PCB-28, 52, 101, 118, 138, and 153, in concrete and caulk from two areas. For the first area, concrete #1, concentrations were obtained by chiseling at five depths. For the second area (concrete #2), concentrations were obtained at four depths into the concrete, with two repetitions (labeled A and B); and in each repetition, sampling was performed in two ways — by chiseling and by drilling. The depth ranges for each of the samples are not stated — only a single depth is provided for each measurement, although some finite depth of concrete must have been sampled.[4] The original analysis used an approximation to the mathematical model that was admittedly invalid for most of the concrete samples, so the following analysis was performed using the exact solution given above (with L set to infinity). It was assumed that in each set of measurements for each PCB congener, the deviations of the measurements from the mathematical model were random in nature, with a lognormal distribution with standard deviation equal to the quadrature sum of the estimated measurement error (20%, as given in the supplementary information) and an additional error term. With this assumption, a loglikelihood for the measurements could be constructed, and maximized to estimate the model parameters K, D, and the additional error term.[5] This approach also allows applying likelihood ratio tests to evaluate the

[3] Apparently Liu *et al*. (2015) were not aware of the second form for the solution, which makes their use of an approximation unnecessary.

[4] Subsequent analysis showed negligible change in the conclusions derived here when plausible depth ranges were used in place of point estimates of depth.

[5] Liu *et al*. (2015), and possibly other authors they cite, appear to have believed that the difficulties in previous estimation of parameters like K and D in other experiments were due to the non-linear nature of the solutions of the differential equation given above. This is false, however. Those difficulties were due entirely to the nature of the measurements made in those other experiments, which inherently could not separate some combination of K and D – see, for example, the discussion below of Guo *et al*. (2012). In this experiment, however, K and D can be readily distinguished.

Green Toxicology LLC www.GreenToxicology.com 781-316-1685 Crouch@GreenToxicology.com

consistency of relationships between the parameters estimated for concrete #1 and the four measurements in concrete #2, and of correlations between parameters and molar masses or other properties of the congeners.

With these assumptions, the estimates of *K* and *D* obtained (for each congener separately) using either chisel or drill for concrete #2A and #2B are not statistically distinguishable ($p = 0.14$ versus distinct values for chisel and drill for each of 2A and 2B), and indeed all the measurements for concrete #2 are consistent with being indistinguishable (for each congener separately) for *K* and *D* ($p = 0.65$ versus distinct values for all four sets of measurements --- the error terms were allowed to vary for each set of measurements). However, concretes #1 and #2 have distinguishable parameters ($p < 4 \times 10^{-6}$). Maximum likelihood estimates for the diffusion coefficient (*D*) and dimensionless mass-fraction-based caulk/concrete partition coefficient (*K*) are shown in Table 1

Table 1 Maximum likelihood estimates for diffusion coefficients and (mass-fraction-based) concrete-caulk partition coefficients evaluated from Liu *et al*. (2015)

	Concrete #1		Concrete #2	
	D (m^2/s)	K	D (m^2/s)	K
PCB-28	6.1E-14	72	9.9E-14	91
PCB-52	5.9E-14	68	8.0E-14	77
PCB-101	5.4E-14	84	6.3E-14	82
PCB-118	5.0E-14	100	5.9E-14	76
PCB-138	5.8E-14	197	6.9E-14	17
PCB-153	2.6E-14	45	8.3E-14	84

Following Guo *et al*. (2012), the values of *D* obtained for the six congeners were tested for conformance with a power law relation with molar mass *m*

$$\left(\frac{D_i}{D_0}\right) = \left(\frac{m_0}{m_i}\right)^{\beta} \tag{5}$$

where *i* labels the congener, the label 0 corresponds to a reference congener, and β is an empirical constant with a value expected to be about 6.5 (Guo *et al.*, 2012). The estimates for *D* were consistent ($p = 0.16$) with a power law, but with exponent $\beta = 0.93$, although with a wide confidence interval on β (at least from 0.6 to 1.4). With this constraint, the estimated diffusion coefficients and (mass-fraction-based) concrete-caulk partition coefficients are given in Table 2. Comparison with Table 1 indicates considerable uncertainty remains when extrapolating between individual congeners using the molar-mass-based power law, although the homolog averages are likely to have smaller uncertainties.

Green Toxicology LLC www.GreenToxicology.com 781-316-1685 Crouch@GreenToxicology.com

Table 2 Diffusion coefficients and (mass-fraction-based) concrete-caulk partition coefficients evaluated from Liu *et al*. (2015), constrained by a power-law dependence of D on molar mass.

	Concrete #1		Concrete #2	
	D (m^2/s)	K	D (m^2/s)	K
PCB-28	6.4E-14	83	8.9E-14	79
PCB-52	5.7E-14	61	7.9E-14	77
PCB-101	5.1E-14	71	7.1E-14	100
PCB-118	5.1E-14	110	7.1E-14	105
PCB-138	4.7E-14	97	6.5E-14	16
PCB-153	4.7E-14	161	6.5E-14	60

The characteristic absorption depth ($2\sqrt{(Dt)}$) after 40 years for this situation ranges from about 1.5 to 2.1 cm, so that the deepest measurements (near 5 cm depth) were at concentrations less than 1/1000 of the surface concentration. A considerable part of the uncertainties involved in fitting the model of equation (4) comes from systematic errors. The measured concentrations near the surface are uniformly higher than expected with the model, although deeper concentrations appear to be better fitted. Such systematic errors are presumably due to deviations of the actual concrete from the idealized model version; in particular, it is plausible that the diffusivity near the surface differs from that deeper in the concrete.

Concrete/air partition coefficient

The experiments of Liu *et al*. (2015) allows estimates of the caulk-concrete partition coefficient K. While the caulk was in direct contact with the concrete, it is plausible that movement of PCBs from the caulk to concrete may have been by vapor transport. If that is the case, then the air-concrete partition coefficient may be derived from the caulk-concrete partition coefficient using the vapor pressures of the PCB congeners above the caulks (since both the caulk and concrete would be in equilibrium with vapor).

The relative concentrations of the six measured congeners in the caulk are most similar to Aroclor 1248, compared with other measured Aroclors (Frame 1997, 1999). Assuming a similar fraction to Aroclor 1248 of the congeners in the PCB mixture[6] used for the caulk implies a total PCB mixture concentration of between 19% and 41% by mass for the caulk adjacent to concrete #1, and between 5% and 33% by mass for the caulk adjacent to concrete #2. Such large mass fractions imply that the PCB mixture was probably the only binding agent used with otherwise inert materials to form the caulks. If so, the vapor pressures above the caulks would correspond with those above a pure PCB mixture.

Making these assumptions, and using the Aroclor 1248 composition provided by Frame (1997) but modified to have the same relative congener compositions for the six congeners measured in the caulks (and the total for these six equal to the total measured in Aroclor 1248), vapor pressures for the six congeners at 20 °C above the caulk were estimated using Raoult's law and saturated vapor pressure

[6] The PCB mixture used in these Danish buildings may not have been an Aroclor, but since the PCB manufacturing processes were likely similar the relative congener compositions would also be similar.

Green Toxicology LLC www.GreenToxicology.com 781-316-1685 Crouch@GreenToxicology.com

estimates from Fischer et al. (1992).[7] Combining these vapor pressures with the concentrations estimated at the surface of the concrete from the analysis for diffusivity (described above), together with an approximate estimate of 2.2 g/cc for the bulk density of concrete, leads to the estimates for concrete/air partition coefficients given in Table 3. These concrete/air partition coefficients (K_m) are expected to be consistent with a power law relationship with vapor pressure of the form discussed by Guo et al. (2012):

$$\left(\frac{K_{mi}}{K_{m0}}\right) = \left(\frac{P_0}{P_i}\right)^{\alpha} \quad (6)$$

where subscript i labels congeners, with 0 being the reference congener, P is vapor pressure, and α is an empirical constant of about 0.5 – 1.0. While the estimates in Table 3 exhibit an increasing trend with increasing molar mass, those for Concrete #1 are consistent with such a power law, those for Concrete #2 are not ($p < 0.0002$, testing both concretes to show the same power law with no power law constraint on the diffusivities).

Table 3 Concrete/air partition coefficient estimates (K_m, concentration-based) derived from Liu *et al.* (2015)

	Concrete #1	Concrete #2
PCB-28	4.8E+05	1.8E+05
PCB-52	1.1E+06	4.7E+05
PCB-101	4.5E+06	2.2E+06
PCB-118	9.1E+06	5.8E+06
PCB-138	9.8E+06	5.5E+07
PCB-153	4.3E+07	1.1E+07

The estimates of Table 3 thus do not show the expected behavior, calling into question the assumptions going into their derivation (in particular, that vapor transport explains the transfer of PCBs from the caulk to the concrete, and/or equilibrium of either the caulk or the concrete with vapor concentrations above pure PCB mixtures).

To obtain independent estimates for concrete/air partition coefficients, the results of Guo *et al*. (2012) were re-analyzed. Guo *et al*. (2012) attempted to evaluate both D and K_m from experiments that measured the cumulative absorption of PCB vapors into concrete samples over approximately 500 hours. To analyze their results, Guo *et al*. (2012) used a correlation derived by Deng *et al*. (2010) as a small-time approximation to the solution to the diffusion equation for the following situation:

- A constant, measured, concentration supplied at constant volume flow rate
- into a fixed volume, well-mixed, chamber with inert, non-adsorbing walls
- containing (only) a fixed mass, solid, flat slab of absorbing material, with
- the non-absorbed vapor exhausted at the concentration in the chamber.

The analysis, and the derived correlation, then related the total quantity of vapor absorbed by the absorbing material to the inlet concentration under these conditions. However, the experiments and

[7] Using Method B of this source, to maintain consistency with the analysis of Guo *et al*. (2012); Method B uses chromatographic column retention times to indirectly estimate vapor pressures. While this method has been rejected for vapor pressure estimation if more direct measurements are available (Li *et al*., 2003), it may provide better extrapolations between congeners for partition coefficients, since the retention time depends on a partition between vapor and column materials.

Green Toxicology LLC www.GreenToxicology.com 781-316-1685 Crouch@GreenToxicology.com

analysis performed by Guo *et al*. (2012) violated several of the assumptions going into the correlations of Deng *et al*. (2010), at least two in non-trivial ways. First, the chamber in Guo *et al*. (2012) had considerable adsorption potential,[8] at least early in the experiment, so that initially the chamber adsorbed approximately 2/3 of the PCB vapors entering it (no data are shown for the effect of the chamber alone at later times). Second, the experiments were conducted with multiple different specimens within the chamber at the same time. Third, parts of each specimen were removed at intervals during the experiment, so that the quantity of each specimen in the chamber was not fixed throughout the experiment. Fourth, at least for the concrete samples, the experimental parameters lay outside the ranges specified by Deng *et al*. (2010) for their correlations. Finally, Guo *et al*. (2012) applied the correlation as though each specimen was present alone in the chamber throughout the experiment, and used the measured average chamber concentration rather than the inlet concentration.

In fact, under the conditions analyzed by Deng *et al*. (2010), the chamber concentration would initially have been zero, and should then have risen towards the inlet concentration. In Guo *et al*. (2012) the chamber concentration is not reported (and may not have been measured) during the first 85 hours, but subsequently was approximately constant at about 1/5 the inlet concentration from hour 85 through 498. This behavior is impossible to explain under the stated conditions of the experiment — all the samples should initially have been absorbing most strongly, with a subsequent decrease of absorption; any adsorption to the chamber walls or absorption by other enclosed components would presumably be limited in time and/or decrease or at least not increase with time; and samples were removed from the chamber at intervals, presumably also decreasing the absorption rate. Similar PCB vapor sources (cut up pieces of caulk) had previously been measured to produce an approximately constant inlet concentration in similar experiments.

Under conditions of constant chamber concentration, the analysis described by equations (1) through (4) adequately describe the absorption of vapors by the concrete samples used by Guo *et al*. (2012) — the effective absorption depth is very small so the shape of the samples is practically irrelevant. For a chamber concentration C_a, the flux at time t into the sample can be obtained from the second expression in equation (4) (substituting the appropriate concentration and partition coefficient term) as

$$K_m C_a \sqrt{\frac{D}{\pi t}} \left\{ 1 + 2 \sum_{n=1}^{\infty} (-1)^n \exp\left[-\left(\frac{Ln}{2\sqrt{Dt}} \right)^2 \right] \right\} \tag{7}$$

The effect of the finite size of the samples is governed by the effective depth L where the flux drops to zero (essentially in the middle of the sample). For the concrete samples used by Guo et al. (2012), L was estimated to be 0.21 cm or larger. At the end of the experiment, at 506 hours, with a diffusivity of about 6×10^{-14} m^2/s the absorption depth $2\sqrt{(Dt)}$ is about 0.066 cm, so the sum in equation (7) is less than 10^{-4}, and much smaller for shorter times. The relative error in treating the integral of the flux as

$$2 K_m C_a \sqrt{\frac{Dt}{\pi}} \tag{8}$$

(*i.e.* omitting the entire summation term in equation (7)) is thus less than 10^{-4}, which is far smaller than the relative errors in fitting models of this nature to the observations (standard deviations of 12% to 50%). Any attempt to extract D separately from the combination $K_m\sqrt{D}$ using measurements of

[8] The chamber included a small computer cooling fan intended to ensure good mixing. The fan used appears from Figures 4.6 and 4.7 of Guo *et al*. (2012) to be made of plastic (as is usual for such fans) that would presumably have been a good PCB absorber.

cumulative flux would thus require high precision measurements that were not subject to any systematic errors, or measurements taken over much longer time scales; and neither condition is met in Guo *et al*. (2012).

Applying equation (8) to the observations[9] of Guo *et al*. (2012) allows estimation of the product $K_m\sqrt{D}$ for the congeners measured, and then using the estimates of D obtained from Liu *et al*. (2015) using the molar-mass-based power law extrapolation between congeners (equation (5) and Table 2) gives the estimates of K_m shown in Table 4 (PCB-105 was measured in the experiment, but the chamber concentration is not documented). For these estimates, the diffusivity measured in concrete #1 of Liu *et al.* (2015) was used. The model for the integral of the flux provided by equation (8) systematically deviates from the observations (it is too high early on, and too low later); but the model adopted by Guo *et al.* (2012) systematically deviates in the same way.[10] These deviations are presumably due to physical effects not incorporated in the model development.

Table 4 Estimates of K_m for concrete derived from experiment S-3 of Guo *et al*. (2012).

	D (m^2/s)	K_m
PCB-17	6.4E-14	2.0E+06
PCB-52	5.7E-14	5.9E+06
PCB-66	5.7E-14	1.1E+07
PCB-101	5.1E-14	1.0E+07
PCB-105	5.1E-14	NA
PCB-110	5.1E-14	1.3E+07
PCB-118	5.1E-14	1.5E+07
PCB-154	4.7E-14	1.0E+07

The estimates of K_m generally increase as vapor pressure decreases, as expected. Although they do not accurately conform ($p = 0.019$) to the power-law dependence on vapor pressure (equation (6)) indicated by Guo *et al*. (2012), enforcing such conformance (which gives an exponent β of 0.49) alters the estimates by less than a factor of 1.5 (Table 5). This power-law dependence, using the vapor pressure estimates of Fischer *et al*. (1992), is used to extrapolate to other congeners, and then to the homolog groups of Aroclor 1242 as an example.[11]

[9] Guo *et al*. (2012) do not tabulate the results of the experiments. However, the document provides vector-based graphics for the chamber concentrations in Figure 6.6 and results for experiment S-3 (which included one concrete sample) in Figure 6.2, allowing extraction of digitized data from the Postscript page-description language of the Portable Document Format (PDF) file. By comparison of the values obtained from the two versions of the graphics (one on a log scale, one on a linear scale), and by comparison with other graphics, the values obtained by this procedure correspond to the original measurements to much better than 1%, well below the measurement accuracy.
[10] The correlation used by Guo *et al*. (2012), derived by Deng *et al*. (2010), has the cumulative flux increasing as $t^{0.61}$ rather than the $t^{0.5}$ of equation (8).
[11] The same approach may be used for other Aroclors, and might be appropriately used in cases where only homolog group measurements are available.

781-316-1685
Green Toxicology LLC www.GreenToxicology.com Crouch@GreenToxicology.com

Table 5 Estimates of K_m for concrete derived from experiment S-3 of Guo *et al*. (2012), enforcing a power-law behavior with vapor pressure.

	D (m^2/s)	K_m
PCB-17	6.4E-14	2.1E+06
PCB-52	5.7E-14	4.0E+06
PCB-66	5.7E-14	7.3E+06
PCB-101	5.1E-14	8.9E+06
PCB-105	5.1E-14	NA
PCB-110	5.1E-14	1.2E+07
PCB-118	5.1E-14	1.7E+07
PCB-154	4.7E-14	1.3E+07

The extrapolation to homolog groups uses the Aroclor 1242 composition documented by Frame (1997), combined with the vapor pressure estimates of Fischer *et al*. (1992; Method B, see footnote 7). Vapor pressures for 27 of the 103 congeners present in Aroclor 1242, and comprising 3% by weight, are missing from the Method B list in Fischer et al. (1992); for these an interpolation based on the other congeners present in Aroclor 1242 was performed. The interpolation used the molecular descriptors (Table 6) of Hansen *et al*. (1999) to form a linear model for the logarithm of estimated vapor pressure. The homolog group average K_m (Table 7) is then obtained as the weighted average of the K_m for individual congeners, where the averaging weight is the percentage composition of Aroclor 1242.

The K_m estimates of Table 5 and extrapolations from them are preferred to those of Table 3 since they are based on experiments that are known to depend on vapor transfer, rather than speculation on mechanisms of transfer from caulk to concrete. There are systematic differences between the two estimates — Table 8 repeats Table 3, adds the values extrapolated from Table 5, and shows the ratio of the latter values to the median of the estimates for the two concretes in Table 3 — that presumably may be accounted for by such mechanisms.

Table 6 Molecular descriptors (Hansen *et al*., 1999) used to linearly interpolate the logarithm of vapor pressure.

Descriptor	Definition	Range
ORTHO2	Number of chlorines in positions 2 and 2’	0–2
ORTHO26	Number of chlorines in positions 2,2’,6, and 6’	0–4
VIC	Number of chlorines vicinal to an ortho-position	0–4
PARA	Number of chlorines in positions 4 and 4’	0–2
DIF	Difference in number of chlorines between rings	0–5
CHLORO	Number of chlorines in molecule	1–10
Note: the META descriptor (number of chlorines in positions 3,3’,5, and 5’) is equal to CHLORO–PARA–ORTHO26, so is not needed in linear models.		

Green Toxicology LLC www.GreenToxicology.com 781-316-1685 Crouch@GreenToxicology.com

Table 7 Homolog average concrete/air partition coefficients K_m for PCBs.

Homolog	**Homolog average K_m**
Monochlorobiphenyl	7.3E+05
Dichlorobiphenyl	1.4E+06
Trichlorobiphenyl	2.7E+06
Tetrachlorobiphenyl	5.6E+06
Pentachlorobiphenyl	1.1E+07
Hexachlorobiphenyl	2.2E+07
Heptachlorobiphenyl	NA
Octachlorobiphenyl	NA
Nonachlorobiphenyl	NA
Decachlorobiphenyl	NA

Table 8 Comparisons of estimates of concrete/air partition coefficient estimates (K_m)

	Derived from Liu *et al.* (2015)		Derived from Guo *et al.* (2012)	Ratio (see text)
	Concrete #1	Concrete #2		
PCB-28	4.8E+05	1.8E+05	3.2E+06	10.7
PCB-52	1.1E+06	4.7E+05	4.0E+06	5.6
PCB-101	4.5E+06	2.2E+06	8.9E+06	2.8
PCB-118	9.1E+06	5.8E+06	1.7E+07	2.3
PCB-138	9.8E+06	5.5E+07	2.5E+07	1.1
PCB-153	4.3E+07	1.1E+07	2.1E+07	0.9

Diffusion of PCBs in sand

Diffusivity

As described by Jury *et al*. (1983,1984a,b,c; 1990, 1992), diffusivity of a contaminant in soil can be estimated as

$$D = \frac{n_w^{10/3} D_w + n_a^{10/3} D_a H}{n^2(\rho_b K_d + n_w + n_a H)} \tag{9}$$

where the terms are

- n_a Air space volume fraction,
- n_w Water space volume fraction,
- D_w Diffusivity of the contaminant in water,
- D_a Diffusivity of the contaminant in air,
- ρ_b Dry bulk density,
- K_d Contaminant soil/water partition coefficient,
- H Henry's law constant for the contaminant.

The diffusivity of PCBs in air can be accurately estimated using the Fuller-Schettler-Giddings correlation (Fuller *et al*., 1966)

$$D_{ab} = 10^{-7} \frac{T^{1.75}(1/M_a + 1/M_b)^{1/2}}{p[(\sum_a v_i)^{1/3} + (\sum_b v_i)^{1/3}]^2} \quad \mathrm{m^2/s} \tag{10}$$

where the (a,b) subscripts indicate vapors or gases a and b respectively, and the terms are

- D_{ab} Diffusivity of vapor or gas b in vapor or gas a (m^2/s),
- T Absolute temperature (Kelvin),
- M Molecular weight (grams/mole),
- v_i Empirically determined effective additive "diffusion volumes" for elements of a and b (1.98 for H, 16.5 for C, 19.5 for Cl, -20.2 for each heterocyclic or aromatic ring; 20.1 for air),
- p Pressure in atmospheres.

The diffusivity of PCBs in water may be accurately estimated by using the Hayduk and Laudie correlation (Hayduk & Laudie, 1974).[12]

$$D_w = \frac{13.26 \times 10^{-9}}{\eta^{1.14} V_B^{0.589}} \quad \mathrm{m^2/s} \tag{11}$$

where the terms are

- D_w Diffusivity in water (m2/s),
- η Viscosity of water (centipoise),
- V_B LeBas molar volume determined by summing additive increments for each element of the PCB (3.7 for H, 14.8 for C, 24.6 for Cl, -15.0 for each 6-membered ring).

The viscosity of water is accurately represented over the range 0°C to 40°C by the empirical expression (Kestin *et al*., 1978)

$$\log \eta(t) = \log 1.002 + \frac{20-t}{t+96}\{1.2364 - 1.37 \times 10^{-3}(20-t) + 5.7 \times 10^{-6}(20-t)^2\} \tag{12}$$

where η is measured in centipoise and t in °C.

[12] Equation (4) of Hayduk & Laudie (1974) mis-prints the exponent of viscosity as 1.4 instead of the correct 1.14.

781-316-1685
Green Toxicology LLC www.GreenToxicology.com Crouch@GreenToxicology.com

Henry's law constants for PCB homologs may be estimated using the correlations of Li *et al*. (2003).

Sand/air partition coefficient

The partition coefficient between bulk sand and air is obtained as (using the previous notation)

$$K_m = \frac{\rho_b K_d + n_w + n_a H}{H} \tag{13}$$

Sand/water partition coefficient

Soil/water partition coefficients for PCBs are generally based on the organic carbon content of the soil, using an estimate for the organic carbon to water (K_{oc}) partition coefficient. However, sand may potentially have very low organic carbon content. To account for this possibility, the sand/water partition coefficient for PCBs in sands with very low organic carbon content is evaluated here and may be used as a conservative estimate in general.

It has been noted that although PCBs sorb to the organic carbon in soil, they also sorb directly to the inorganic component of soil (Delle Site, 2001; Paya-Perez *et al*., 1991; Lee *et al.*, 1979), so that in general the soil/water partition coefficient (K_d) can be written

$$K_d = K_0 + K_{oc} f_{oc} \tag{14}$$

where f_{oc} is the organic carbon fraction in the soil. Typical values for K_{oc} for PCBs are in the range 10^5 to 10^6 L/kg, whereas K_0 ranges up to a few thousand (Paya-Perez *et al.*, 1991), so that soil organic carbon contents of order 0.01% should have K_d dominated by the inorganic sorption.

Lee *et al*. (1979) published measurements on a sand containing less than 0.01% organic carbon for multiple PCB congeners, 16 of which were uniquely identified. The measurements were in the form of experimental concentrations of dissolved PCBs, the concentrations attained when this solution was allowed to equilibrate in a blank vessel, and the concentrations attained after equilibration in a similar vessel containing a known amount of sand. Paya-Perez *et al*. (1991) provide mean and standard deviation results from 3 evaluations of K_d for 19 identified PCB congeners for a soil with 0.03% organic carbon. Cortes *et al*. (1991) provide evaluations of K_d for 6 identified PCB congeners for a soil with 0.03% organic carbon. Evaluation of $K_d = K_0$ from these experiments required the subtraction of measured concentrations, together with a blank correction, so that the results were obtained from a difference in relatively large numbers. For the less chlorinated congeners, with smaller values of K_d, this could result in estimates that were negative (*e.g.* all Lee *et al*.'s estimates for the monochlorobiphenyls were negative).

To estimate K_0 for all the PCB congeners in Aroclor 1242 (used as an example here), the measurements were incorporated in a model in which the logarithm of K_0 was estimated as a linear combination of the molecular descriptors of Hansen *et al*. (1999; see Table 6), with a normal error term for K_0 (not Log(K_0)) in which the standard deviation of the estimate was assumed to be a constant plus a term proportional to K_0, to account for the expected nature of experimental errors (including the possibility of negative results). Of the 41 results[13] mentioned in the last paragraph, 38 were incorporated in the model (the three negative monochlorobiphenyl results from Lee *et al*., 1979, were omitted as providing no useful information). It was found that the DIF molecular descriptor provided no statistically significant useful information, so it was dropped from the model. The final maximum likelihood model coefficients are

[13] There is some overlap in the congeners measured by the three authors (*e.g*. all measured PCB-52), so that only 37 congeners are included in the list of 41 results.

Green Toxicology LLC www.GreenToxicology.com 781-316-1685 Crouch@GreenToxicology.com

shown in Table 9, and the measured versus estimated values for 37 results are shown in Figure 1. The two apparent outliers from the linear curve (at small values of Log(K_o)) have standard deviation estimates that exceed their value, so they contribute very little information and are not in fact outliers, while the 38th measurement was negative, but again the standard deviation estimate is sufficiently large that it is not an outlier.

Table 9 Coefficients for the molecular descriptor model for Log(K_0).

Descriptor	Coefficient
ORTHO2	0.294256
ORTHO26	-0.21073
VIC	0.199088
PARA	0.134202
CHLORO	0.270208
Constant	1.378993

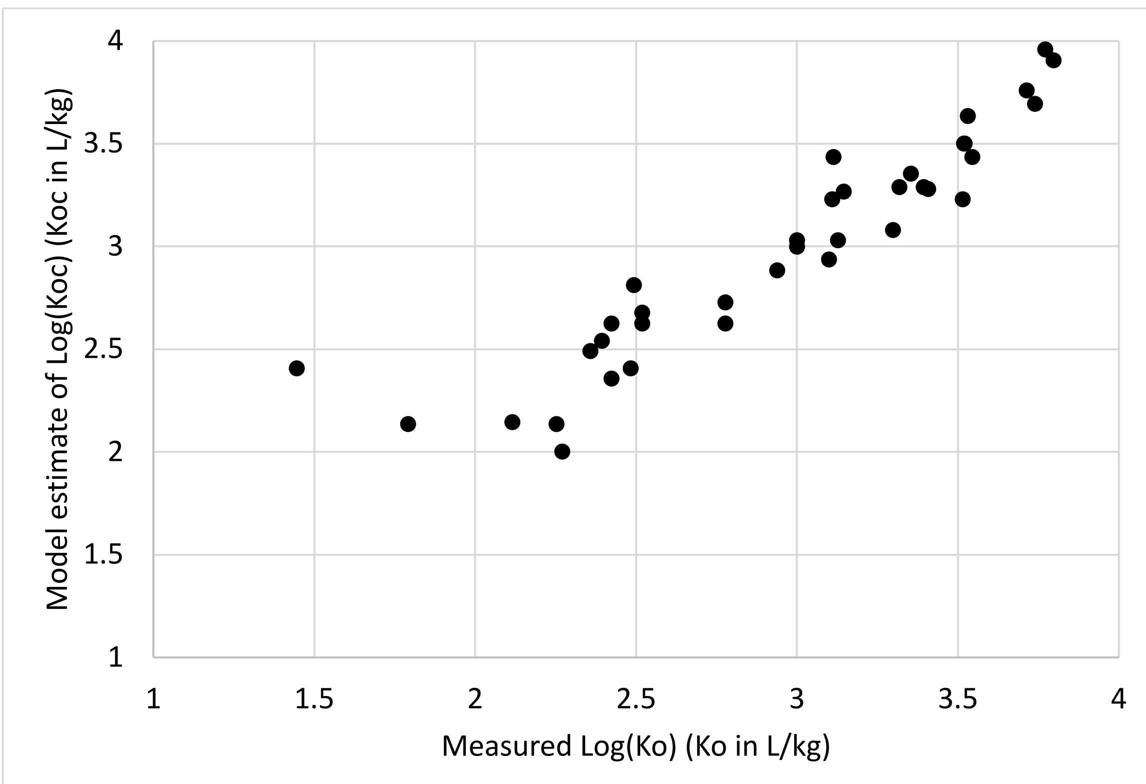

Figure 1 Measured and model estimated K_0

To obtain average K_0 estimates for the homolog groups of Aroclor 1242, the model was used to estimate K_0 for each of the congeners in Aroclor 1242, and weighted averages over the homolog groups were calculated using the mass fractions measured by Frame (1997). These homolog averages are shown in Table 10.

Table 10 PCB homolog average K_0 estimates based on the model fit to 41 measured congeners.

	K_0 estimate
Monochlorobiphenyl	55
Dichlorobiphenyl	131
Trichlorobiphenyl	277
Tetrachlorobiphenyl	601
Pentachlorobiphenyl	1358
Hexachlorobiphenyl	3422
Heptachlorobiphenyl	NA
Octachlorobiphenyl	NA
Nonachlorobiphenyl	NA
Decachlorobiphenyl	NA

References

Cortes A, Riego J, Paya-Perez AB, Larsen B. Soil sorption of co-planar and non-planar PCBs. Toxicol Environ Chem. 1991;31(1):79-86.

Delle Site A. Factors Affecting Sorption of Organic Compounds in Natural Sorbent/Water Systems and Sorption Coefficients for Selected Pollutants. A Review. J Phys Chem Ref Data 2001;30(1):187–439.

Deng Q, Yang X, Zhang JS. New indices to evaluate volatile organic compound sorption capacity of building materials (RP-1321). HVAC&R Res 2010;16(1):95–105.

Fischer RC, Wittlinger R, Ballschmiter K. Retention-index based vapor pressure estimation for polychlorobiphenyl (PCB) by gas chromatography. Fresenius J Anal Chem. 1992;342(4):421–425.

Frame GM. A collaborative study of 209 PCB congeners and 6 Aroclors on 20 different HRGC columns. 2. Semi-quantitative Aroclor congener distributions. Fresenius J Anal Chem. 1997;357(6):714–722.

Frame GM. Improved Procedure for Single DB-XLB Column GC-MS-SIM Quantitation of PCB Congener Distributions and Characterization of Two Different Preparations Sold as "Aroclor 1254". J High Resol Chromatogr. 1999;22(10):533–540.

Fuller EN, Schettler PD, Giddings JC. A new method for prediction of binary gas-phase diffusion coefficients. Ind Eng Chem. 1966;58(5):18–27.

Guo Z, Liu X, Krebs KA, Greenwell DJ, Roache NF, Stinson RA, Nardin JA, Pope RH. Laboratory study of polychlorinated biphenyl (PCB) contamination and mitigation in buildings. Part 2. Transport from primary sources to building materials and settled dust. EPA/600/R-11/156A. January 2012. https://clu-in.org/download/contaminantfocus/pcb/PCB-lab-studies-2.pdf.

Hansen BG, Paya-Perez AB, Rahman M, Larsen BR. QSARs for K_{OW} and K_{OC} of PCB congeners: A critical examination of data, assumptions and statistical approaches. Chemosphere 1999 Dec;39(13):2209–2228.

Hayduk W, Laudie H. Prediction of diffusion coefficients for nonelectrolytes in dilute aqueous solutions.

Green Toxicology LLC www.GreenToxicology.com 781-316-1685 Crouch@GreenToxicology.com

AIChE J. 1974 May;20(3):611–615.

Jury WA, Russo D, Streile G, El Abd H. Correction to "Evaluation of volatilization by organic chemicals residing below the soil surface." Water Resources Research. 1992;28(2):607–608.

Jury WA, Russo D, Streile G, El Abd H. Evaluation of volatilization by organic chemicals residing below the soil surface. Water Resources Research. 1990;26(1):13–20.

Jury WA, Spencer WF, Farmer WJ. Behavior assessment model for trace organics in soil, I. Model description. J Environ Qual. 1983;12(4):558–564.

Jury WA, Spencer WF, Farmer WJ. Behavior assessment model for trace organics in soil, II. Chemical classification parameter sensitivity. J Environ Qual. 1984a;13(4):467–572.

Jury WA, Spencer WF, Farmer WJ. Behavior assessment model for trace organics in soil, III. Application of screening model. J Environ Qual 1984b;13(4):573–579.

Jury WA, Spencer WF, Farmer WJ. Behavior assessment model for trace organics in soil, IV. Review of experimental evidence. J Environ Qual. 1984c;13(4):580–586.

Kestin J, Sokolov M, Wakeham WA. Viscosity of liquid water in the range −8°C to 150°C. J Phys Chem Ref Data. 1978;7(3):941–948.

Lee MC, Griffin RA, Miller ML, Chian ESK. Adsorption of water-soluble polychlorinated biphenyl aroclor 1242 and used capacitor fluid by soil materials and coal chars. J Environ Sci Health Part A. 1979;14(5):415-442.

Li N, Wania F, Lei YD, Daly GL. A Comprehensive and Critical Compilation, Evaluation, and Selection of Physical–Chemical Property Data for Selected Polychlorinated Biphenyls. J Phys Chem Ref Data. 2003;32(4):1545–1590.

Liu C, Kolarik B, Gunnarsen L, Zhang Y. C-Depth Method to Determine Diffusion Coefficient and Partition Coefficient of PCB in Building Materials. Environ Sci Technol. 2015;49(20):12112–12119. http://dx.doi.org/10.1021/acs.est.5b03352. (With supplemental information).

Paya-Perez AB, Riaz M, Larsen BR. 1991. Soil sorption of 20 PCB congeners and six chlorobenzenes. Ecotoxicology and environmental safety, 1991;21(1):1–17.

Appendix 1. Efficient computation of common diffusion cases

Commonly occurring situations where computationally efficient solutions of the time-dependent diffusion equation are needed for diffusion of one material into another. Most references provide solutions that are computationally efficient only for either small or large times, but generally there are mathematical transformations that allow efficient computation in either extreme.

1-dimensional slab, finite or infinite thickness, constant diffusivity, constant concentration faces

Assume an infinite (*y*, *z* directions) flat slab with thickness *L* in the *x* direction, initially with zero concentration of diffusate throughout [equivalently, a finite (y, z) such slab but with impermeable *y*, *z* edges]. Set the concentration (mass per unit volume) *C* at one surface (*x* = 0) to a constant value C_0 at time *t* = 0 and maintain that concentration for all time, while the concentration at the other surface (*x* = *L*) is kept at zero. Assume a constant diffusivity *D* within the slab. Then we have

$$\frac{\partial C}{\partial t} = D\frac{\partial^2 C}{\partial x^2} \tag{15}$$

with boundary conditions

$$\begin{gathered} C(x, t = 0) = 0 \\ C(x = 0,\ \text{all } t) = C_0 \\ C(L, \text{all } t) = 0 \end{gathered} \tag{16}$$

The Laplace transform

$$\tilde{C}(x,s) = \int_0^\infty C(x,t)\exp(-st)\,dt \tag{17}$$

of the solution has the form

$$\tilde{C}(x,s) = \frac{C_0}{s}\frac{\sinh\sqrt{\frac{s}{D}}(L-x)}{\sinh\sqrt{\frac{s}{D}}L} \tag{18}$$

Define dimensionless parameters

$$\begin{aligned} \alpha &= x/L \quad \text{so } 0 \le \alpha \le 1 \\ \gamma &= \sqrt{\frac{Dt}{L^2}} \quad \text{so } \gamma \ge 0 \end{aligned} \tag{19}$$

The first (α) is just the fractional distance into the slab, while the second (γ) is the ratio of a characteristic diffusion distance to the slab dimension. With these definitions, the solution may be expressed in the two forms:

$$\begin{aligned} C(x,t) &= C_0\left\{(1-\alpha) - 2\sum_{n=1}^{\infty}\frac{\sin(n\pi\alpha)\exp(-n^2\pi^2\gamma^2)}{n\pi}\right\} \\ &= C_0\left\{\text{erfc}\left(\frac{\alpha}{2\gamma}\right) + \sum_{n=1}^{\infty}\left[\text{erfc}\left(\frac{n+\alpha/2}{\gamma}\right) - \text{erfc}\left(\frac{n-\alpha/2}{\gamma}\right)\right]\right\} \end{aligned} \tag{20}$$

Green Toxicology LLC www.GreenToxicology.com 781-316-1685 Crouch@GreenToxicology.com

where the first form is appropriate for numerical calculation at large times (large γ), the second form at small times (small γ), since each series converges most rapidly in those respective neighborhoods. The flux (mass per unit area per unit time)

$$F(x,t) = -D\frac{\partial C}{\partial x} \tag{21}$$

at any depth ($x = \alpha L$) into the slab may be similarly expressed in the two forms:

$$\begin{aligned} F(x,t) &= \frac{DC_0}{L}\left\{1 + 2\sum_{n=1}^{\infty}\cos(n\pi\alpha)\exp(-n^2\pi^2\gamma^2)\right\} \\ &= C_0\sqrt{\frac{D}{\pi t}}\sum_{n=-\infty}^{\infty}\exp\left[-\left(\frac{n+\alpha/2}{\gamma}\right)^2\right] \end{aligned} \tag{22}$$

where again numerical calculation at large times is most appropriate with the first form, and at small times with the second.

The cumulative flux (mass per unit area)

$$G(x,t) = \int_0^t F(x,w)\,dw \tag{23}$$

through any plane within the slab may also be expressed in two forms:[14]

$$\begin{aligned} G(x,t) &= C_0L\left\{\gamma^2 + \frac{3(1-\alpha)^2-1}{6} - 2\sum_{n=1}^{\infty}\frac{\cos(n\pi\alpha)\exp(-n^2\pi^2\gamma^2)}{n^2\pi^2}\right\} \\ &= 2C_0\sqrt{\frac{Dt}{\pi}}\left\{\sum_{n=0}^{\infty}\exp\left(-\left(\tfrac{n+\alpha/2}{\gamma}\right)^2\right)\left[1 - 2\tfrac{n+\alpha/2}{\gamma}\mathrm{M}\left(\tfrac{n+\alpha/2}{\gamma}\right)\right]\right. \\ &\qquad\left. + \sum_{n=1}^{\infty}\exp\left(-\left(\tfrac{n-\alpha/2}{\gamma}\right)^2\right)\left[1 - 2\tfrac{n-\alpha/2}{\gamma}\mathrm{M}\left(\tfrac{n-\alpha/2}{\gamma}\right)\right]\right\} \end{aligned} \tag{24}$$

where

$$M(x) = \exp(x^2)\int_x^{\infty}\exp(-t^2)dt = \frac{\sqrt{\pi}}{2}\exp(x^2)\,\mathrm{erfc}(x) \tag{25}$$

is Mills ratio. As before, the first expression Is numerically most appropriate for large times, the second for small times. It is also possible to express the second form in equation (24) in terms of the incomplete gamma function with argument –½ (for example, by directly integrating the second form of equation (22), or by expressing erfc as an incomplete gamma function with argument ½ and using the recurrence relation for incomplete gamma functions).

For infinite L, both α and γ vanish, but their ratio remains finite, as do the products $L\alpha$ and $L\gamma$. In that case, only the n = 0 term of the second forms of equations (20), (22), and (24) survive and provide compact and readily computable solutions for all times (while the first forms become indeterminate or converge very slowly).

[14] Note the different lower limits on the sums in the second form.

Green Toxicology LLC www.GreenToxicology.com 781-316-1685 Crouch@GreenToxicology.com

1-dimensional slab, finite thickness, constant diffusivity, constant concentration and impermeable barrier faces

Assume an infinite (*y*, *z* directions) flat slab of uniform diffusivity with thickness *L* in the *x* direction, initially with zero concentration throughout (equivalently, a finite (y, z) such slab but with impermeable *y*, *z* edges). This is the configuration examined using approximate solutions by Liu *et al*. (2015); the following analysis renders those approximations unnecessary. Set the concentration *C* at one surface ($x = 0$) to a constant value C_0 at time $t = 0$ and maintain that concentration for all time, while the other surface ($x = L$) forms an impermeable barrier (this is equivalent to the situation in which a similar slab of thickness 2*L* has both surfaces maintained at constant concentration). Once again, equation (15) governs the evolution of the concentration, and we seek solutions satisfying boundary conditions:

$$\begin{gathered} C(x, t=0) = 0 \\ C(x=0,\ \text{all } t) = C_0 \\ \left.\frac{\partial C}{\partial x}\right|_{(x=L,\ \text{all } t)} = 0 \end{gathered} \tag{26}$$

The Laplace transform of the solution has the form

$$\tilde{C}(x,s) = \frac{C_0}{s} \frac{\cosh \sqrt{\frac{s}{D}}(L-x)}{\cosh \sqrt{\frac{s}{D}} L} \tag{27}$$

and with the same definitions as equation (19) the solution takes the forms:

$$\begin{aligned} C(x,t) &= C_0 \left\{ 1 - 2 \sum_{n=1}^{\infty} \frac{\sin\big((n-0.5)\pi\alpha\big) \exp(-(n-0.5)^2\pi^2\gamma^2)}{(n-0.5)\pi} \right\} \\ &= C_0 \left\{ \operatorname{erfc}\left(\frac{\alpha}{2\gamma}\right) + \sum_{n=1}^{\infty} (-1)^n \left[\operatorname{erfc}\left(\tfrac{n+\alpha/2}{\gamma}\right) - \operatorname{erfc}\left(\tfrac{n-\alpha/2}{\gamma}\right) \right] \right\} \end{aligned} \tag{28}$$

while the flux is given by:

$$\begin{aligned} F(x,t) &= 2\frac{DC_0}{L} \sum_{n=1}^{\infty} \cos\big((n-0.5)\pi\alpha\big) \exp(-(n-0.5)^2\pi^2\gamma^2) \\ &= C_0 \sqrt{\frac{D}{\pi t}} \sum_{n=-\infty}^{\infty} (-1)^n \exp\left[-\left(\frac{n+\alpha/2}{\gamma}\right)^2 \right] \end{aligned} \tag{29}$$

and the cumulative flux by:

$$\begin{aligned} G(x,t) &= C_0 L \left\{ 1 - \alpha + 2 \sum_{n=1}^{\infty} \frac{\cos\big((n-0.5)\pi\alpha\big) \exp(-(n-0.5)^2\pi^2\gamma^2)}{(n-0.5)^2\pi^2} \right\} \\ &= 2C_0 \sqrt{\frac{Dt}{\pi}} \left\{ \sum_{n=0}^{\infty} (-1)^n \exp\left(-\left(\tfrac{n+\alpha/2}{\gamma}\right)^2 \right) \left[1 - 2\tfrac{n+\alpha/2}{\gamma} \mathrm{M}\left(\tfrac{n+\alpha/2}{\gamma}\right) \right] \right. \\ &\qquad \left. + \sum_{n=1}^{\infty} (-1)^n \exp\left(-\left(\tfrac{n-\alpha/2}{\gamma}\right)^2 \right) \left[1 - 2\tfrac{n-\alpha/2}{\gamma} \mathrm{M}\left(\tfrac{n-\alpha/2}{\gamma}\right) \right] \right\} \end{aligned} \tag{30}$$

Green Toxicology LLC   www.GreenToxicology.com   781-316-1685
Crouch@GreenToxicology.com

As for the second form of equation (24) (see above), the second form of equation (30) may be expressed in terms of the incomplete gamma function with argument –½ .

Again, for infinite L both α and γ vanish but their ratio remains finite, as do the products $L\alpha$ and $L\gamma$. In that case, only the n = 0 term of the second forms of equations (28), (29) and (30) survive and provide the same compact and readily computable solutions for all times as the same limit applied to equations (20), (22), and (24) (while again the first forms become indeterminate or converge very slowly).

1-dimensional slab within an enclosure with constant flow into the enclosure

This is the experimental situation modeled by Deng *et al*. (2010). A homogeneous flat slab of specimen material, initially free of the diffusate material, with thickness 2L, and with edges assumed to be impermeable (or a sufficiently large slab transverse to the thickness to allow that assumption with negligible error), is supported in an impermeable and non-absorbing enclosure of volume V with inlet and exhaust vents. The support is such that air has free access to both slab surfaces of total area A. Air containing the diffusate at concentration C_0 is blown into the enclosure at constant rate Q, starting at time t = 0, kept well-mixed within the enclosure, and exhausted from the enclosure with a diffusate concentration $C_a(t)$ equal to that in the enclosure. Under these conditions, it is assumed that the accessible surfaces of the slab are kept at a diffusate concentration KC_a where K is a constant slab-to-air partition coefficient.

Using a coordinate system with x-axis perpendicular to the slab, with x = 0 at the surface of the slab, $x > 0$ within the slab, and letting $C(x,t)$ be the concentration of diffusate in the slab at depth x into the slab ($0 \le x \le L$), the governing equations for diffusion of the diffusate into the slab are then:

$$\begin{aligned}
D\frac{\partial^2 C}{\partial t^2} &= \frac{\partial C}{\partial t} \\
QC_0 &= QC_a - AD\left.\frac{\partial C}{\partial x}\right|_{x=0} + V\frac{dC_a}{dt} \\
C(0,t) &= KC_a \\
C(x,0) &= 0 \\
\left.\frac{\partial C}{\partial t}\right|_{x=L} &= 0 \\
C_a(t) &= 0 \text{ for } t \le 0
\end{aligned} \tag{31}$$

(for $L \le x \le 2L$ the physical symmetry gives $C(x,t)=C(2L-x,t)$; the situation is also equivalent to a similar slab of total area A, with just the side x = 0 exposed and an impermeable barrier at $x = L$.)
Defining dimensionless parameters p, q by:

$$\begin{aligned}
p &= \frac{QL}{ADK} \\
q &= \frac{V}{AKL}
\end{aligned} \tag{32}$$

and continuing to use the notation of equation (19), the Laplace transform for C with a general time-varying input concentration C_0 is given by

Green Toxicology LLC www.GreenToxicology.com 781-316-1685 Crouch@GreenToxicology.com

$$\tilde{C}(x,s) = pK\frac{\tilde{C}_0(s)\cosh\sqrt{\frac{sL^2}{D}}(1-\alpha)}{\left(p+q\frac{sL^2}{D}\right)\cosh\sqrt{\frac{sL^2}{D}}+\sqrt{\frac{sL^2}{D}}\sinh\sqrt{\frac{sL^2}{D}}} \tag{33}$$

where the tilde indicates a Laplace transform.

Since this is a product of transforms, its inverse (the solution $C(x,t)$) may be written as a convolution integral in the form written by Deng *et al*. (2010):

$$C(x,t) = \frac{2Q}{AL}\sum_{n=0}^{\infty}\left\{\frac{\lambda_n^2\cos\left(\lambda_n(1-\alpha)\right)}{[p+(q+1)\lambda_n^2+(p-q\lambda_n^2)^2]\cos(\lambda_n)}\int_0^t C_0(\tau)\exp\left[-\frac{\lambda_n^2 D(t-\tau)}{L^2}\right]d\tau\right\} \tag{34}$$

where

$$\begin{gathered} p-q\lambda_n^2 = \lambda_n\tan\lambda_n \qquad n=0,1,2,3,\cdots \\ 0<\lambda_0<\pi/2 \\ (n-1/2)\pi<\lambda_n<(n+1/2)\pi \qquad n>0 \end{gathered} \tag{35}$$

Note that equations (34) and (35) are written in terms of dimensionless parameters (α, p, q, λ_n) rather than the parameters (x, α, β, λ_n) of Deng *et al*. (2010) that have dimensions of length, inverse length, length, inverse length respectively; and that the coordinate system is inverted relative to that of Deng *et al*. (2010). Equation (35) may be solved rapidly and accurately using the methodology of Appendix 2.

Specializing equation (34) to a fixed influent concentration C_0 gives

$$C(x,t) = 2pKC_0\sum_{n=0}^{\infty}\frac{\cos\left(\lambda_n(1-\alpha)\right)[1-\exp(-\lambda_n^2\gamma^2)]}{\cos(\lambda_n)[p+(q+1)\lambda_n^2+(p-q\lambda_n^2)^2]} \tag{36}$$

again using notation from equation (19), with corresponding flux through a plane at $x = \alpha L$ of

$$F(x,t) = 2pKC_0\frac{D}{L}\sum_{n=0}^{\infty}\frac{\lambda_n\sin\left(\lambda_n(1-\alpha)\right)[\exp(-\lambda_n^2\gamma^2)-1]}{\cos(\lambda_n)[p+(q+1)\lambda_n^2+(p-q\lambda_n^2)^2]} \tag{37}$$

and cumulative flux past that plane (obtained by directly integrating equation (37)) of

$$G(x,t) = 2pKC_0L\gamma^2\sum_{n=0}^{\infty}\frac{\lambda_n\sin\left(\lambda_n(1-\alpha)\right)\left[\frac{1-\exp(-\lambda_n^2\gamma^2)}{\lambda_n^2\gamma^2}-1\right]}{\cos(\lambda_n)[p+(q+1)\lambda_n^2+(p-q\lambda_n^2)^2]} \tag{38}$$

Dividing $G(0,t)$ (*i.e.* equation (38) with $\alpha = 0$ and using equation (35)) by the ultimate cumulative flux KC_0L gives the sorption saturation degree (*SSD*) of Deng *et al*. (2010), expressed in completely dimensionless form as

$$SSD = 2p\gamma^2\sum_{n=0}^{\infty}\frac{(p-q\lambda_n^2)\left[\frac{1-\exp(-\lambda_n^2\gamma^2)}{\lambda_n^2\gamma^2}-1\right]}{[p+(q+1)\lambda_n^2+(p-q\lambda_n^2)^2]} \tag{39}$$

which is equivalent to the expression given by Deng *et al*. (2010). Unfortunately, equations (36) through (39) are practically unusable numerically in the forms given, because they converge extremely slowly (*e.g.* equation (39) converges as $1/n^2$ for large n) for both large and small times. While convergence speed-up methods can be applied, there is a more direct approach that gives practical series.

Instead of using the convolution form of equation (34), the Laplace transform of the input concentration may be used in equation (33) and the result inverted directly, effectively allowing analytic summation of the slowly converging parts of equations (36) through (39). With a constant influent concentration C_0, its Laplace transform is C_0/s. Substituting in equation (33) and inverting gives

$$C(x,t) = KC_0\left\{1 - 2p\sum_{n=0}^{\infty}\frac{\cos\big(\lambda_n(1-\alpha)\big)\exp(-\lambda_n^2\gamma^2)}{\cos(\lambda_n)\,[p+(q+1)\lambda_n^2+(p-q\lambda_n^2)^2]}\right\} \tag{40}$$

with flux

$$F(x,t) = 2pKC_0\frac{D}{L}\sum_{n=0}^{\infty}\frac{\lambda_n\sin\big(\lambda_n(1-\alpha)\big)\exp(-\lambda_n^2\gamma^2)}{\cos(\lambda_n)\,[p+(q+1)\lambda_n^2+(p-q\lambda_n^2)^2]} \tag{41}$$

and cumulative flux (obtained by inverting the Laplace transform for the integral of the flux, which is just $1/s$ times the Laplace transform for the flux itself, rather than direct integration of equation (41))

$$G(x,t) = KC_0L\left\{1-\alpha - 2p\sum_{n=0}^{\infty}\frac{\sin\big(\lambda_n(1-\alpha)\big)\exp(-\lambda_n^2\gamma^2)}{\lambda_n\cos(\lambda_n)\,[p+(q+1)\lambda_n^2+(p-q\lambda_n^2)^2]}\right\} \tag{42}$$

so that

$$SSD = 1 - 2p\sum_{n=0}^{\infty}\frac{(p-q\lambda_n^2)\exp(-\lambda_n^2\gamma^2)}{\lambda_n^2[p+(q+1)\lambda_n^2+(p-q\lambda_n^2)^2]} \tag{43}$$

Equations (40) through (43) are rapidly convergent and numerically practical for large times (and in particular equation (43) is probably sufficient for all relevant times in practical applications). For sufficiently small times, however, they would require an impractical number of terms (and roundoff error might dominate calculations). As for the previous two physical situations analyzed, it is possible to derive series that converge rapidly at small times, although they are more involved.

Define

$$\begin{aligned}
S(n,x) &= \frac{1}{p-qx^2+ix}\left(\frac{p-qx^2-ix}{p-qx^2+ix}\right)^n\\
I(n,m) &= \frac{1}{\pi i}\int_{-\infty}^{\infty}\exp(-u^2)\,S\left(n,\frac{1}{\gamma}\left(u-i\frac{n+\alpha/2}{\gamma}\right)\right)\frac{1}{\left(u-i\frac{n+\alpha/2}{\gamma}\right)^m}du\\
J(n,m) &= \frac{1}{\pi i}\int_{-\infty}^{\infty}\exp(-u^2)\,S\left(n-1,\frac{1}{\gamma}\left(u-i\frac{n-\alpha/2}{\gamma}\right)\right)\frac{1}{\left(u-i\frac{n-\alpha/2}{\gamma}\right)^m}du
\end{aligned} \tag{44}$$

where as usual $i = \sqrt{-1}$, then

$$\frac{C(x,t)}{KC_0} = p\left\{\sum_{n=0}^{\infty}\exp\left[-\left(\frac{n+\alpha/2}{\gamma}\right)^2\right]I(n,1) + \sum_{n=1}^{\infty}\exp\left[-\left(\frac{n-\alpha/2}{\gamma}\right)^2\right]J(n,1)\right\} \tag{45}$$

$$\frac{F(x,t)}{KC_0D/L} = \frac{ip}{\gamma}\left\{\sum_{n=0}^{\infty}\exp\left[-\left(\frac{n+\alpha/2}{\gamma}\right)^2\right]I(n,0) - \sum_{n=1}^{\infty}\exp\left[-\left(\frac{n-\alpha/2}{\gamma}\right)^2\right]J(n,0)\right\} \tag{46}$$

$$\frac{G(x,t)}{KC_0L} = -ip\gamma\left\{\sum_{n=0}^{\infty}\exp\left[-\left(\frac{n+\alpha/2}{\gamma}\right)^2\right]I(n,2) - \sum_{n=1}^{\infty}\exp\left[-\left(\frac{n-\alpha/2}{\gamma}\right)^2\right]J(n,2)\right\} \tag{47}$$

Green Toxicology LLC www.GreenToxicology.com 781-316-1685 Crouch@GreenToxicology.com

These expressions have been written using complex numbers for simplicity of notation, and where necessary (for $n = 0$, $\alpha = 0$) the contours of integration in equation (44) should be considered to be slightly below the real axis. Despite this, all results are real. [Proof: the complex expressions occurring within the integrals are the product of the exponential term, which is real and even in u, and ratios of polynomials which can be expressed as polynomials in iu with real coefficients when the initial constants in equations (44), (46) and (47) are included. All imaginary terms can thus be expressed as products of odd powers of u with expressions even in u, hence are antisymmetric in u, and all such antisymmetric terms vanish by the symmetry of the integrals.]

The most interesting of these formulae is the last, where the right hand side evaluated at $\alpha = 0$ is just the *SSD* defined above. Writing

$$r_1 = \frac{1+\sqrt{1-4pq}}{2q} \qquad r_2 = \frac{1-\sqrt{1-4pq}}{2q}$$
$$s_3 = i\frac{\alpha}{2\gamma} \qquad s_1 = s_3 + i\gamma r_1 \qquad s_2 = s_3 + i\gamma r_2 \tag{48}$$

and using the complex error function

$$\begin{aligned} w(z) &= \exp(-z^2)\operatorname{erfc}(-iz) && \text{for all } z \\ &= \sum_{n=0}^{\infty} \frac{(iz)^n}{\Gamma\left(\frac{1}{2}n+1\right)} && \text{for all } z \\ &= \frac{1}{\pi i}\int_{-\infty}^{\infty} \frac{\exp(-u^2)}{u-z}\,du && \text{for } \mathcal{Im}(z) > 0 \end{aligned} \tag{49}$$

the $n = 0$ term in equation (47) may be written as

$$-\frac{w(s_3)}{p} + 2\gamma\left(\frac{1}{\sqrt{\pi}} + is_3 w(s_3)\right) + \frac{r_2}{r_1(r_2-r_1)}w(s_1) + \frac{r_1}{r_2(r_1-r_2)}w(s_2) \tag{50}$$

which then gives, on setting $\alpha = 0$

$$SSD = -\frac{1}{p} + \frac{2\gamma}{\sqrt{\pi}} + \frac{r_2}{r_1(r_2-r_1)}w(i\gamma r_1) + \frac{r_1}{r_2(r_1-r_2)}w(i\gamma r_2) + O(\exp(-1/\gamma^2)) \tag{51}$$

This gives a practical evaluation of *SSD* for $\gamma < 0.15$, so that omitted terms are of order $\exp(-1/\gamma^2) < 5 \times 10^{-20}$. At this value of γ, equation (43) only needs about 15 terms to reach the same level of precision, so is quite practical to use for larger γ. If in addition $4pq < 1$, then r_1 and r_2 are real, so that the arguments of the *w* functions in equation (51) are pure imaginary, and the *w* functions may be readily evaluated using the first line of equation (49). If $4pq > 1$, the 3rd and 4th terms on the right side of equation (51) (involving the *w* function) are complex conjugates, so their sum is real.

Equation (51) may also be expanded in powers of γ using the second line of equation (49). Writing

$$T_0 = {}^1\!/_p; \quad T_1 = -1; \quad T_{n+1} = -\frac{1}{q}(T_n + pT_{n-1}) \text{ for } n > 0 \tag{52}$$

then

$$SSD = \sum_{n=3}^{\infty} \frac{\gamma^n T_n}{\Gamma\left(\frac{1}{2}n+1\right)} + O(\exp(-1/\gamma^2)) \tag{53}$$

so that initially SSD increases as γ^3 (*i.e.* as $t^{3/2}$). Equation (53) is only useful computationally if $|\gamma r_1|$ is sufficiently small.

781-316-1685
Green Toxicology LLC www.GreenToxicology.com Crouch@GreenToxicology.com

Appendix 2. Solving an auxiliary equation

Computing the terms of the series in equations (34) through (43) requires solving:

$$p - qx^2 = x \tan x \quad \text{with} \;\; p > 0, q > 0 \tag{54}$$

in positive values of *x*. A sketch comparing each side of this equation

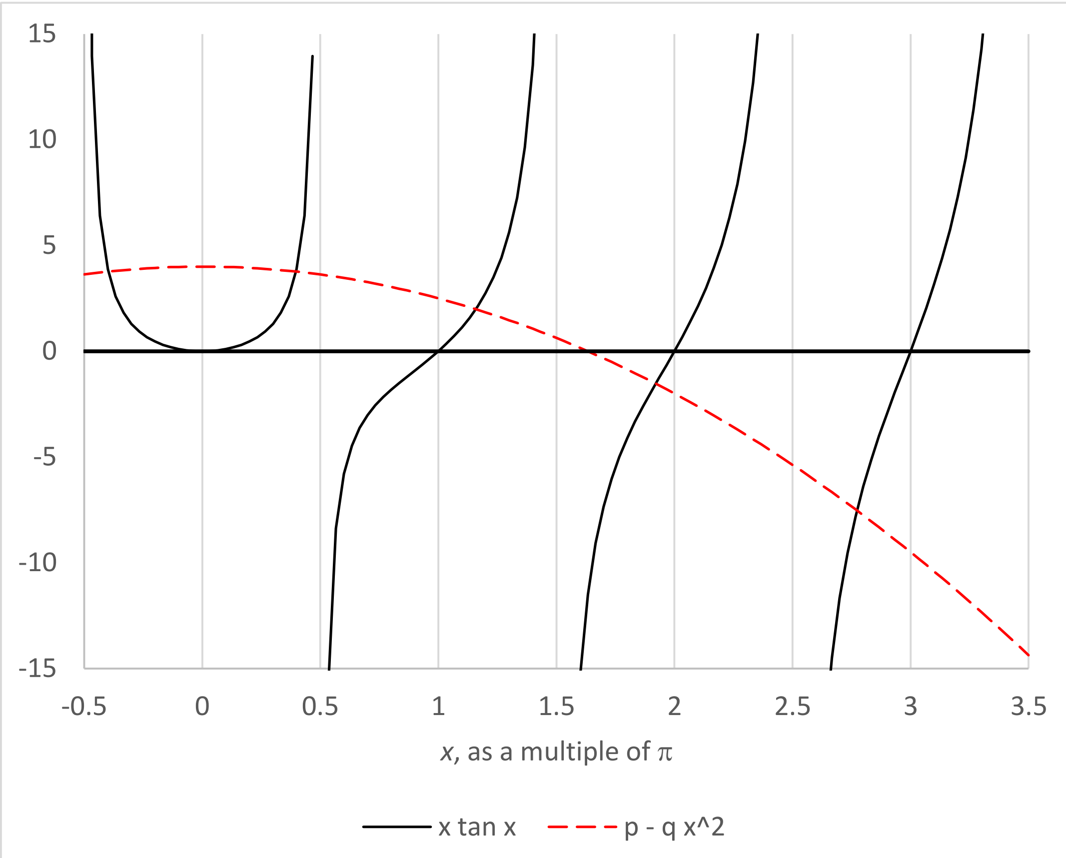

Figure 2 Sketch of each side of equation (54). The intersections of the curves are solutions.

shows that the positive solutions satisfy

$$\begin{gathered} x = \lambda_n \qquad\qquad n = 0,1,2,3,\cdots \\ 0 < \lambda_0 < \pi/2 \\ (n - 1/2)\pi < \lambda_n < (n + 1/2)\pi \qquad n > 0 \end{gathered} \tag{55}$$

and that

$$\lambda_n \longrightarrow (n - 1/2)\pi \quad \text{as} \quad n \longrightarrow \infty \tag{56}$$

An effective solution method is to choose an initial estimate as shown below, then perform Halley iteration. For $n = 0$ set $x = \theta$ and approximate $\tan\theta$ by

$$\begin{gathered} \tan\theta \approx \frac{\theta(1 - \gamma\theta^2)}{1 - \beta\theta^2} \quad -\frac{\pi}{2} \le \theta \le \frac{\pi}{2} \\ \text{with} \qquad \beta = \frac{4}{\pi^2}, \;\; \gamma = \beta(1 - 2\beta) \end{gathered} \tag{57}$$

Those choices for β and γ ensure the correct (first) pole position and residue for the approximation to the tangent, and give a good approximation over the indicated range. Substituting this approximation in equation (54) with $x = \theta$ leads to a quadratic in θ^2, and hence (choosing the correct root, and expressing it in a numerically stable way) gives the initial estimate

781-316-1685
Green Toxicology LLC www.GreenToxicology.com Crouch@GreenToxicology.com

$$\theta_0 \simeq \sqrt{\frac{2p}{p\beta + q + 1 + \sqrt{(p\beta - q - 1)^2 + 8p\beta^2}}} \tag{58}$$

For $n > 0$, set $x = n\pi + \theta$ and get an initial estimate θ_0 from the intersection of the tangents at $x = n\pi$ to the left and right sides of equation (54):

$$\theta_0 = \frac{p - qn^2\pi^2}{n\pi(1 + 2q)} \tag{59}$$

If $|\theta_0| \leq C$, it is accurate enough to use as an initial approximation. Empirically, a cutoff value of $C = 0.25$ is adequate. Otherwise,

(a) if $\theta_0 > +C$, set

$$x = (n + 0.5)\pi - \delta \tag{60}$$

with $\delta > 0$ and solve

$$\begin{aligned} p - q[(n + 0.5)\pi - \delta]^2 \quad &= [(n + 0.5)\pi - \delta] \tan[(n + 0.5)\pi - \delta] \\ &= [(n + 0.5)\pi - \delta] \cot \delta \\ &= [(n + 0.5)\pi - \delta] \frac{1 - \delta^2/3}{\delta} + O(\delta^3) \end{aligned} \tag{61}$$

Setting

$$\begin{aligned} u &= p - q(n + 0.5)^2\pi^2 + 1 \\ v &= (n + 0.5)\pi \end{aligned} \tag{62}$$

gives, to second order in δ,

$$v(2q + 1/3)\delta^2 + u\delta - v = 0 \tag{63}$$

with solutions

$$\delta = \frac{-u \pm \sqrt{u^2 + 4v^2(2q + 1/3)}}{2v(2q + 1/3)} \tag{64}$$

To select the required positive root the + sign has to be chosen, and then stable numerical calculation requires

$$\begin{aligned} \text{if } u \geq 0 \quad \delta &= \frac{2v}{u + \sqrt{u^2 + 4v^2(2q + 1/3)}} \\ \text{else} \quad \delta &= \frac{-u + \sqrt{u^2 + 4v^2(2q + 1/3)}}{2v(2q + 1/3)} \end{aligned} \tag{65}$$

Then the initial estimate for $\theta = x - n\pi$ is given by

$$\theta_0 = 0.5\pi - \delta \tag{66}$$

(b) If instead $\theta_0 < -C$, exactly the same type of analysis as in (a) with

$$\begin{aligned} u &= p - q(n - 0.5)^2\pi^2 + 1 \\ v &= (n - 0.5)\pi \end{aligned} \tag{67}$$

leads to

$$\begin{aligned} \text{if } u \geq 0 \quad \theta_0 &= -0.5\pi + \frac{u + \sqrt{u^2 + 4v^2(2q + 1/3)}}{2v(2q + 1/3)} \\ \text{else} \quad \theta_0 &= -0.5\pi + \frac{2v}{-u + \sqrt{u^2 + 4v^2(2q + 1/3)}} \end{aligned} \tag{68}$$

With the initial estimate for θ_0 so obtained, Halley iteration

781-316-1685
Green Toxicology LLC www.GreenToxicology.com Crouch@GreenToxicology.com

$$\Delta\theta = -f/(f' - ff''/(2f')) \tag{69}$$

on

$$\begin{gathered} x = \theta + n\pi \\ f(\theta) = (p - qx^2)\cos\theta - \theta\sin\theta \end{gathered} \tag{70}$$

gives double precision accuracy within 3 iterations, usually 2 iterations, for all *p*, *q*.

Green Toxicology LLC www.GreenToxicology.com 781-316-1685 Crouch@GreenToxicology.com